Calculation of the electronic structure and the linear optical response of the Sb - and $Sn - Si(111)\sqrt{3} \times \sqrt{3}$ surfaces

1996 J. Phys.: Condens. Matter 8 6585

(http://iopscience.iop.org/0953-8984/8/36/011)

J. Phys.: Condens. Matter **8** (1996) 6585–6596. Printed in the UK

Calculation of the electronic structure and the linear optical response of the Sb– and Sn–Si(111)$\sqrt{3} \times \sqrt{3}$ surfaces

H T Anyele† and C C Matthai‡

† Departamento de Física, Centro Tecnológico, Universidade Federal do Maranhão, São Luís, CEP 67383-360, Brazil

‡ Department of Physics and Astronomy, University of Wales College of Cardiff, PO Box 913, Cardiff CF2 3YB, UK

Received 23 April 1996

Abstract. A self-consistent tight-binding technique has been employed to calculate the electronic structures of the Sb– and Sn–Si(111)$\sqrt{3} \times \sqrt{3}$ surfaces. For the Sn reconstructed surface, two filled and one unfilled surface states as well as one straddling the Fermi level were calculated. Three filled and two unfilled surface states were calculated for the Sb reconstructed surface. These surface state positions are in good agreement with experiments. We have also calculated the imaginary part of the surface dielectric function, ϵ_2, the surface dielectric function anisotropy and the corresponding reflectance anisotropy spectra for these reconstructed surfaces. For comparison we have also calculated the difference between the imaginary parts of the surface dielectric functions for the Sn–Si(111)$\sqrt{3} \times \sqrt{3}$ and Si(111)$\sqrt{3} \times \sqrt{3}$ surfaces.

1. Introduction

Optical techniques probe the details of electronic structure since the response of electronic states to electromagnetic fields is so directly related to the electronic structure. The response of a solid to light (i.e. absorption and/or reflection) is measured in terms of the dielectric function that has a real part (ϵ_1) and an imaginary part (ϵ_2) which are related by the Kramers–Kronig relations [1]. The imaginary (absorptive) part at each energy depends on the density of occupied and empty states as well as on the momentum matrix elements [2]. There are principally two main contributions to the dielectric constant: an electronic and a lattice contribution. For high frequencies in comparison to the natural vibrational frequencies of most lattices, which are usually in the infrared region of the electromagnetic spectrum, the lattice contribution can be neglected. Hence the low-frequency limit here will correspond to frequencies small compared to characteristic electron excitation frequencies, but still well above the vibrational frequencies.

The search for more powerful techniques used for probing surface chemistry, structural and electronic properties has encountered serious limitations because most techniques involve the use of electrons or ion beams forbidding their use in high-pressure growth chambers. It has recently been demonstrated that changes in the dielectric function resulting from an epilayer as thin as one monolayer on a substrate can be measured using ellipsometry [3]. Reflection anisotropy spectroscopy (RAS) is another optical technique that has been shown to be useful in the monitoring of growth of semiconductors by MBE and also

0953-8984/96/366585+12$19.50

in the high-pressure environment of MOVPE [4, 5]. RAS examines the difference in reflectivity for light of two orthogonal polarizations incident on the surface. The difference in reflectivity which is a consequence of the anisotropy of the surface electronic structure is highly dependent on the surface atomic configuration and chemistry. It has been shown that the RAS signal depends on the photon energy and can be used to fingerprint particular surface structures. For example, the GaAs (2×4) As-rich reconstructed surface has a particular identifiable camel-shaped RAS spectrum, whereas the (4×2) Ga-rich surface has an altogether different shape [6]. It has further been shown that some of the features in the spectra may be ascribed to the presence of dimers on these surfaces [7]. It is quite clear then, that information relating to the detailed nature of the surface bonds may be extracted from the RAS data by correlating them with detailed calculations of the surface states and corresponding optical response. However, to fully exploit the potential of this technique, it is important to study a few test systems both experimentally and theoretically. The Si and GaAs reconstructed surfaces are examples of such systems which have been studied [8–11] to date. Near-monolayer coverages of Sb and Sn on Si(111) provide another such system and are the subject of this paper.

Until the advent of angle-resolved and momentum-resolved photoelectron spectroscopy, the experimental determination of band structures relied principally on ϵ_2-measurements. In atoms and molecules, absorption reflects very directly the differences in energies between different, sharply defined levels, and the resulting absorption lines can be used directly to declare 'term values' which may be thought of as one-electron energy values for the atoms and molecules. In solids, the sharp spectral absorption lines are replaced by bands, and though it is not possible to work back to determine the bands from the spectrum, it is possible to extract specific energy differences between bands.

The joint density of states (JDOS) is known to provide a useful approximation to ϵ_2, but its assumption of equal momentum matrix elements for all transitions is very simplistic. It can be shown by symmetry that matrix elements connecting certain wave functions vanish; e.g. the matrix elements connecting two band states of Γ_1 symmetry is zero just as it is for s states of the free atoms. ϵ_2 is more accurately determined by calculating the momentum matrix elements explicitly using electronic wave functions. These wave functions can be obtained by one of numerous self-consistent electronic structure calculation methods. Techniques which use density functional theory are known to give an error in the calculated band gap [12] and consequently the position of the electronic surface states may be incorrect. Although the band-gap error can be easily accounted for, the contribution from the surface states may be harder to correct.

In this work, the self-consistent tight-binding (SCTB) method in the extended Hückel approximation has been used to provide a description of the surface electronic structure of the Sn– and Sb–Si(111)$\sqrt{3} \times \sqrt{3}$ surfaces. The SCTB is an empirical scheme which takes into account charge transfer at the surface and provides a good description of the surface electronic structure. This method has been used before to calculate surface state positions and to study Fermi level pinning in the As–Si(100)2×1 surface [13] and the $NiSi_2$–Si(111) interface [14]. The calculated surface state positions in the band gap were in excellent agreement with experiments.

In section 2 the theory of the calculations is presented and section 3 provides the method of calculation. In section 4 the results are presented and discussed accordingly. Conclusions are given in section 5.

2. Theory of the calculation

Tight-binding methods are increasingly being used to investigate problems in condensed matter physics. This is no doubt due to the local description of the problem which is physically appealing and in addition gives deep insight into the nature of the chemical bonds at or near the surface. In the SCTB technique, the one-electron wave functions are written in the form [15, 16]

$$\psi_i(k, r) = (B_i(k))^{-1/2} \sum_{\alpha s} C_{\alpha s}(k, i)\Phi_{\alpha s}(k, r) \tag{1}$$

where the Bloch functions $\Phi_{\alpha s}(k, r)$ are taken to be linear combinations of atomic valence orbitals and are given by

$$\Phi_{\alpha s}(k, r) = N^{-1/2} \sum_{l} \exp(-\mathrm{i}\boldsymbol{k} \cdot \boldsymbol{R}_{ls})\phi_\alpha(r - R_{ls}) \tag{2}$$

where α = valence orbital type, s = basis atom index, i = band index, N = number of unit cells in the crystal, $\boldsymbol{R}_{ls}$ = position of atom number s in the lth unit cell.

The atomic orbital functions, $\phi_\alpha(r)$, are taken to be Slater-type functions with exponents η_α. The η_α are parametrized to fit the bulk band structures of the different elemental species [15, 16]. Substituting for ψ in the one-electron Schrödinger equation leads to the secular equation

$$|H_{\alpha s,\beta t}(k) - E_i(k)S_{\alpha s,\beta t}(k)| = 0 \tag{3}$$

where $H_{\alpha s,\beta t}(k)$ and $S_{\alpha s,\beta t}(k)$ are respectively matrix elements of the effective Hamiltonian and the overlap matrix between the two Bloch functions $\Phi_{\alpha s}(k)$ and $\Phi_{\beta t}(k)$. The main approximation in this technique is that the diagonal matrix elements of the Hamiltonian are given by the negative of the valence orbital ionization potential $I_{\alpha s}$. The off-diagonal elements are obtained by relating $I_{\alpha s}$ to the overlap matrix elements involving matrix elements, namely

$$H_{\alpha s,\beta t} = -0.5\, K_{\alpha\beta}(I_{\alpha s} + I_{\beta t})S_{\alpha s,\beta t} \tag{4}$$

where the $K_{\alpha\beta}$ are treated as parameters. For off-diagonal matrix elements involving two different atomic species, s and t, K was taken to be the arithmetic average of those of the two elements, i.e. $\frac{1}{2}(K^s_{\alpha\beta} + K^t_{\alpha\beta})$.

The ionization potentials depend on the charge on the atom and on its electron configuration; thus the problem is solved self-consistently. These ionization potentials are given by

$$I_{\alpha s}(\Delta q_s) = C_{\alpha s} + B_{\alpha s}\Delta q_s + \sum_t R_{st}\Delta q_t \tag{5}$$

where Δq_s is the excess charge on atom s. $C_{\alpha s}$ is the α-orbital energy of the neutral atom in its ground state and $B_{\alpha s}$ is the change in the orbital energy due to deviation from charge neutrality. R_{st} is the Coulomb repulsion integral for the charges on different atoms. The constants C and B are obtained from ionization potentials of neutral and ionized atoms which are available in spectroscopic tables [17].

For wavelengths greater than the interatomic spacing, (i.e. the low-frequency limit) the imaginary part of the dielectric function as obtained from standard perturbation theory [18, 19] is given by

$$\epsilon_2(\omega) = \frac{1}{\pi}\left[\frac{e}{m\omega}\right]^2 \sum_{i,j} \int_{BZ} [P_{ji}P_{ij}\delta(E_{ji} - \hbar\omega) - P_{ij}P_{ji}\delta(E_{ji} + \hbar\omega)]\, \mathrm{d}k \tag{6}$$

where

$$P_{ij}(k) = \langle \psi_i(k)|\boldsymbol{e}\cdot\boldsymbol{P}|\psi_j(k)\rangle. \tag{7}$$

$\boldsymbol{e}$ is a unit vector in the direction of polarization of the light, $\boldsymbol{P}$ is the momentum operator and $E_{ji} = E_j(k) - E_i(k)$. j = unoccupied conduction band index and i = occupied valence band index. Substituting equations (1) and (2) in (7) gives

$$P_{ij}(k) = N^{-1}(B_iB_j)^{-1/2}\sum_{\alpha\beta}\sum_{st} C^v_{\alpha s}C^c_{\beta t}\sum_{R_{ls}R_{mt}}\exp(-\mathrm{i}\boldsymbol{k}\cdot(\boldsymbol{R}_{ls}-\boldsymbol{R}_{mt}))T \tag{8}$$

where

$$T = \langle\phi_\alpha(r-R_{ls})|\boldsymbol{e}\cdot\boldsymbol{P}|\phi_\beta(r-R_{mt})\rangle \tag{9}$$

where v and c refer to the valence and conduction band states respectively (i.e. transitions from valence band states to conduction band states). We can write $\boldsymbol{e}\cdot\boldsymbol{P}$ simply as P and then consider two orthogonal light polarizations. Hence T becomes

$$T = \langle\phi_\alpha(r-R_{ls})|P|\phi_\beta(r-R_{mt})\rangle. \tag{10}$$

Since ϕ_β and ϕ_α are localized (the tight-binding formalism), we can use [18]

$$P = \frac{m\mathrm{i}}{\hbar}[H_0, r] \tag{11}$$

where H_0 is the crystal Hamiltonian, and since we are evaluating

$$\langle\phi_\alpha(r-R_{ls})|[H_0,r]|\phi_\beta(r-R_{mt})\rangle$$

we can add a correction potential $v(r)$ to H_0 such that

$$H_0^1|\phi_\beta\rangle \equiv [H_0+v(r)]|\phi_\beta\rangle = \varepsilon_\beta|\phi_\beta\rangle. \tag{12}$$

Now if we define

$$H_0^2|\phi_\alpha\rangle \equiv [H_0+v^1(r)]|\phi_\alpha\rangle \equiv [H_0+v(r)+\Delta v(r)]|\phi_\alpha\rangle \tag{13}$$

such that $H_0^2|\phi_\alpha\rangle = \varepsilon_\alpha|\phi_\alpha\rangle$ and if we assume that the matrix elements of Δv are small compared to those of H_0^2, we can write

$$\langle\phi_\beta|[H_0,r]|\phi_\alpha\rangle \simeq (\varepsilon_\beta-\varepsilon_\alpha)\langle\phi_\beta|r|\phi_\alpha\rangle. \tag{14}$$

Hence T becomes

$$T = \frac{m\mathrm{i}}{\hbar}[\varepsilon^t_\beta - \varepsilon^s_\alpha]\langle\phi_\beta(r-R_{mt})|r|\phi_\alpha(r-R_{ls})\rangle \tag{15}$$

where ε^t_β and ε^s_α are the energies of the β- and α-orbitals on sites t and s after self-consistency has been achieved.

Assuming that the dipole matrix elements connecting two different atoms can be neglected [8] *(this single-centre integral approximation was tested by evaluating the two-centre integrals and examining their effect on the bulk dielectric function. It was observed that ϵ_2 was affected only in the high-energy regime, i.e. >6 eV, with an enhancement of the amplitude)*, then

$$\langle\phi_\beta(r)|r|\phi_\alpha(r-R) = 0 \qquad \text{for } R\neq 0. \tag{16}$$

Considering also that T is non-zero only for $\varepsilon_\beta \neq \varepsilon_\alpha$, thus T becomes

$$T = \frac{m\mathrm{i}}{\hbar}[\varepsilon^s_\beta - \varepsilon^s_\alpha]\int \phi^s_\beta(r)\phi^s_\alpha(r)r\ \mathrm{d}r. \tag{17}$$

Hence the momentum matrix elements, equation (7), are given by

$$P_{ij}(k) = \frac{m\mathrm{i}}{N\hbar\sqrt{B_iB_j}}\sum_{\alpha\beta}\sum_s [\varepsilon^s_\beta-\varepsilon^s_\alpha]C^v_{\alpha s}(k)C^{c*}_{\beta s}(k)\int\phi^s_\beta(r)\phi^s_\alpha(r)r\ \mathrm{d}r. \tag{18}$$

ϵ_2 was calculated as given by equation (6) using the above expression for $P_{ij}(k)$.

3. The method of calculation

The Sn–Si(111)$\sqrt{3} \times \sqrt{3}$ surface corresponds to 1/3 monolayer (ML) coverage [8, 20, 21] (1 ML is defined as the number of atoms of the ideal substrate, being 7.83×10^{14} atoms cm^{-2} for the Si(111) substrate) with Sn residing at the T_4 sites [22]. The surface atomic positions used were those obtained from surface x-ray diffraction by Conway *et al* [22]. Photoelectron diffraction [23] and both scanning tunnelling microscopy (STM) and first-principles calculation [24] have confirmed a $\sqrt{3} \times \sqrt{3}$ geometry for this coverage with Sb atoms forming trimers on the Sb–Si(111) surface. This corresponds to a full monolayer coverage with the Sb atoms residing near the atop (T_1) sites and bonding directly with a silicon atom beneath the surface and each of the two remaining Sb atoms in the trimer whose centre is at the T_4 site [24]. Thus three out of the five valence electrons of each Sb atom participate in the formation of covalent bonds. The other two occupy lone-pair orbitals which protrude out of the surface.

Table 1. Parameters used to calculate the surface electronic structures. The symbols are given in the text.

Parameter	Si	Sb	Sn
η_s	1.90	2.44	2.31
η_p	1.41	2.00	1.80
C_s	14.95	14.52	14.23
C_p	7.77	8.44	7.01
B_s	12.39	10.45	8.89
B_p	10.13	7.60	7.27
K_{ss}	1.75	2.0	1.52
K_{pp}	1.75	1.52	1.80
K_{sp}	1.46	1.78	1.33

The Slater exponents, η_α, and the constants relating to the overlap matrix of the Hamiltonian, $K_{\alpha\beta}$, were parametrized and fitted to the bulk band structures obtained by Chelikowsky and Cohen [25] using non-local pseudopotentials. Table 1 shows the parameters for Sn and Si obtained from the fitting. Also shown are the parameters for Sb which were obtained from Whittle *et al* [26]. Once this fitting process was completed for the bulk materials, the subsequent parameters were used in the calculation of the electronic structure of the Sb– and Sn–Si(111)$\sqrt{3} \times \sqrt{3}$ surfaces.

Both surfaces were modelled using a periodically repeating slab geometry. For the Sn surface, half of the unit cell consisted of eight silicon layers each containing three atoms, a tin layer with only one atom and three empty (vacuum) layers. These vacuum layers were found to be sufficient to avoid surface interactions. Half of the slab for the Sb surface consisted of eight silicon layers each containing three atoms, an antimony layer with three atoms (trimer atoms) and three vacuum layers.

The imaginary surface dielectric function, ϵ_2^s, was then calculated using the expression

$$\epsilon_2^s = (\epsilon_2^{110} + \epsilon_2^{1\bar{1}2})/2 \tag{19}$$

where ϵ_2^{110} and $\epsilon_2^{1\bar{1}2}$ refer to the components of ϵ_2^s in the [110] and [$1\bar{1}2$] directions. The surface dielectric anisotropy is given by

$$\Delta\epsilon_2^s = (\epsilon_2^{110} - \epsilon_2^{1\bar{1}2})/2 \tag{20}$$

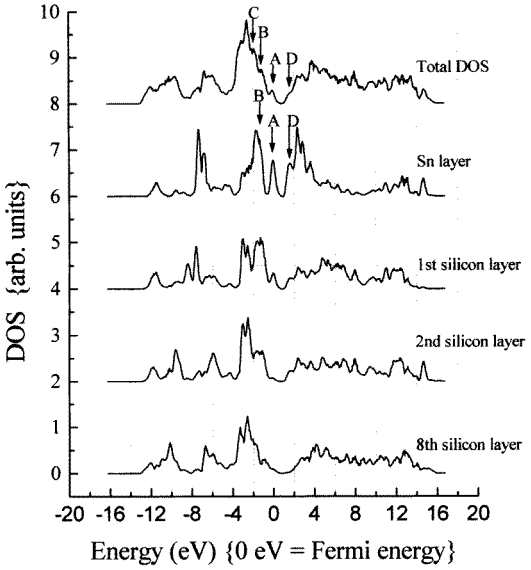

Figure 1. The total and local density of states (DOS) for the Sn–Si(111)$\sqrt{3} \times \sqrt{3}$ slab. Surface states are labelled A, B, C and D.

and can be related to the experimentally measured deflection anisotropy. This is achieved by first performing a Kramers–Kronig transform to give the real part of the dielectric function, ϵ_1, from the knowledge of ϵ_2. The complex dielectric function is related to the real and imaginary parts of the refractive index, n and k respectively, through the relation

$$\sqrt{\epsilon} = n + \mathrm{i}k \qquad \epsilon = \epsilon_1 + \mathrm{i}\epsilon_2. \tag{21}$$

The reflectance at normal incidence is defined as

$$r = \frac{(n-1)^2 + k^2}{(n+1)^2 + k^2} \tag{22}$$

and the reflectance anisotropy is then given by

$$\frac{\Delta r}{r} = \frac{2(r^{110} - r^{1\bar{1}2})}{(r^{110} + r^{1\bar{1}2})}. \tag{23}$$

Aspnes *et al* [27, 28] have shown that the features in the experimentally derived dielectric anisotropy and RAS spectra are virtually the same. This is expected as analysis of the linear response within a three-phase model yields the result

$$\frac{\Delta r}{r} \propto (\epsilon_2^{110} - \epsilon_2^{1\bar{1}2}). \tag{24}$$

For both the electronic density of states and the optical response calculations, the Brillouin zone integration was performed using the tetrahedron method [29]. In this method the irreducible zone is divided into parallelepipeds and is further reduced into six tetrahedra. The contribution to the matrix element from each tetrahedron was evaluated using the Skriver method [29]. Twelve k-points obtained from symmetry considerations were used for the reciprocal-space integration for both surface calculations.

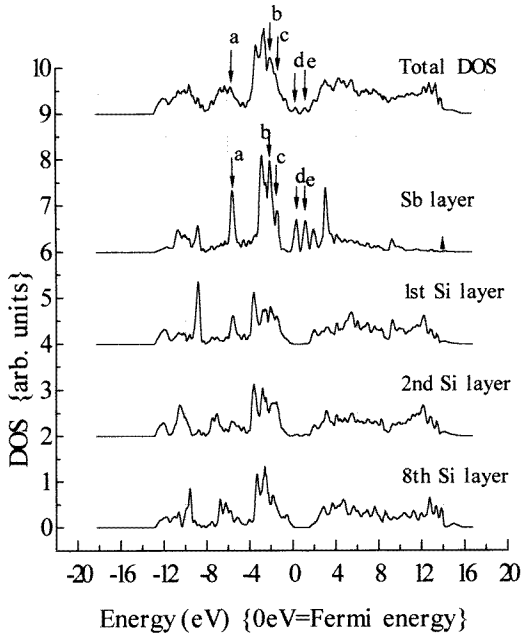

Figure 2. The total and local density of states (DOS) for the Sb–Si(111)$\sqrt{3} \times \sqrt{3}$ slab. Surface states are labelled a, b, c, d and e.

4. Results and discussion

Figure 1 shows the calculated total (T), and local (L) density of states (DOS) for the top three layers as well as one of the bulk-like layers for the Sn reconstructed surface. The main surface states labelled A, B and C occur at the Fermi energy, E_f (i.e. 0 eV), at 1.1 eV and 1.9 eV below E_f respectively. These states were identified as surface states after detailed examination of the coefficients of the wave functions. The greatest contributions to these states were from the surface atoms. These energy positions for surface states are in very good agreement with the angle-resolved ultra-violet photoelectron spectroscopy (ARUPS) study of Kinoshita *et al* [30]. In their study they denoted these states S1, S2 and S3 respectively. We have also identified an unfilled surface state labelled D which occurs at approximately 1.4 eV above E_f.

Figure 2 shows the calculated TDOS and LDOS for the top three layers as well as one of the bulk-like layers for the Sb reconstructed surface. We can immediately identify unfilled surface states labelled d and e at energies 0.4 eV and 1.4 eV above E_f. These are very localized at the surface. These states correspond to the Y- and Z-states observed by Kinoshita *et al* [31] in their momentum-resolved inverse photoemission spectroscopy (KRIPS) study. We have also calculated three other surface states labelled a, b and c. States b and c occur at between 2.0 and 1.3 eV below E_f. These states were observed and denoted A_1 and A_2 by Kinoshita *et al* [30] in their ARUPS study. These states are associated with the lone pairs on the Sb atoms in the trimer model [24]. The filled surface state observed and denoted x by Kinoshita *et al* [31] at about 2.8 eV were not predicted; however, we have identified another deep-lying filled surface state, denoted a, at approximately 5.4 eV below E_f. This state originates on the Sb layer and decays into the bulk of the slab.

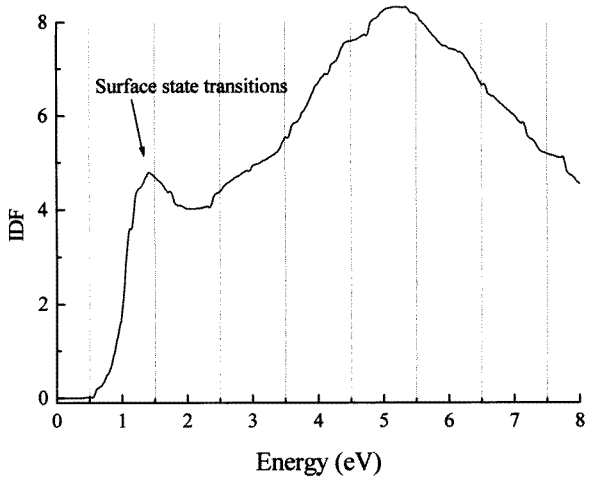

Figure 3. The imaginary part of the dielectric function (IDF), ϵ_2, for the Sn–Si(111)$\sqrt{3} \times \sqrt{3}$ surface.

The good agreement between the calculated surface states and experimental findings prompted the investigation of optical properties of these reconstructed surfaces. In order to gain confidence in our calculations, the imaginary part of the dielectric function as well as the JDOS of bulk silicon were calculated. The JDOS was found to closely resemble ϵ_2. This resemblance is because for bulk, the momentum matrix elements for all transitions are almost equal as assumed in the JDOS approximation. The calculated ϵ_2 agrees reasonably well with experiments [11] and other calculations [32–34] only in the low-energy regime, (i.e. <6 eV), because of the on-site approximation made in equation (16) (i.e. the neglect of near-neighbour interactions). Since we are only interested in the low energies, for large (surface) calculations, the two-centre integrals were neglected.

Figure 3 shows ϵ_2 for the Sn reconstructed surface. In addition to the bulk features, there is a peak at 1.4 eV and a broad feature between 2.5 eV and 3.0 eV which are associated with transitions from surface states labelled A and B to the state labelled D respectively. It was noted that unlike the case for the bulk calculation, the momentum matrix elements for the surface state to surface state transitions were considerably larger than those for other transitions for energies below 3 eV. The JDOS (not shown) confirmed this because the features below 3 eV were almost suppressed. The calculated anisotropy in the surface dielectric function, $\epsilon_2^{110} - \epsilon_2^{1\bar{1}2}$, plotted against energy is shown in figure 4(a). The reflectance anisotropy (i.e. RAS) spectrum calculated from equations (22) and (23) is shown in figure 4(b). As may be observed, the energies of the features in the dielectric anisotropy are the same as those for the RAS. The main features of the spectrum are found to occur between 1.0 eV and 4.5 eV, and from an analysis of the various matrix elements, contributions can be attributed to transitions from occupied to unoccupied surface states arising from silicon atoms in the layer below the surface. Surprisingly although these atoms suffer very small displacements of order 0.01 Å from their equilibrium positions, they appear to make a significant contribution to the RAS signal. In order to calculate the effect of Sn on the $\sqrt{3} \times \sqrt{3}$ surface, the ϵ_2-spectrum for silicon adatoms on the Si(111)$\sqrt{3} \times \sqrt{3}$ surface was calculated after obtaining its electronic structure in the same manner as in [35]. The Si(111)$\sqrt{3} \times \sqrt{3}$ surface is similar to the Sn surface except for the fact that the Si adatom

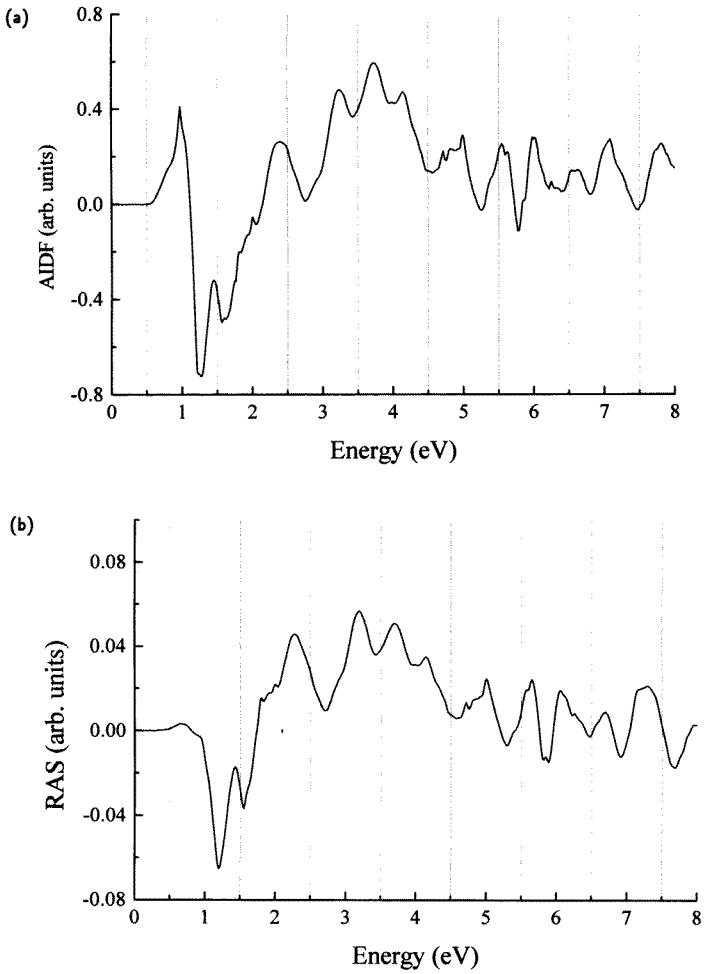

Figure 4. (a) The anisotropy in the imaginary part of the surface dielectric function (AIDF) for the Sn–Si(111)$\sqrt{3} \times \sqrt{3}$ surface as a function of energy. The two orthogonal polarizations considered are along the [110] and [1$\bar{1}$2] directions. (b) The RAS spectrum for the Sn–Si(111)$\sqrt{3} \times \sqrt{3}$ surface.

is replaced by a Sn adatom and of course both surfaces have different relaxations. Thus these surfaces are directly comparable. The difference between the ϵ_2-spectra in shown in figure 5. The main difference peak occurs at about 1.3 eV. The prediction of differences in ϵ_2 can only be confirmed by ellipsometric measurements.

Figure 6 shows the ϵ_2-spectrum as calculated for the Sb reconstructed surface. Two peaks occur at 1.6 eV and 2.1 eV in addition to the bulk features. These correspond to transitions from states labelled b and c in figure 2 to states labelled d and e. These features were barely resolved in the JDOS as in the case of Sn. It should be noted that because the calculations presented here were performed employing a slab configuration, the effect of the adlayers on the substrate would be exaggerated when compared with experiments.

Figure 7(a) shows $\epsilon_2^{110} - \epsilon_2^{1\bar{1}2}$ plotted against energy as calculated for the Sb–

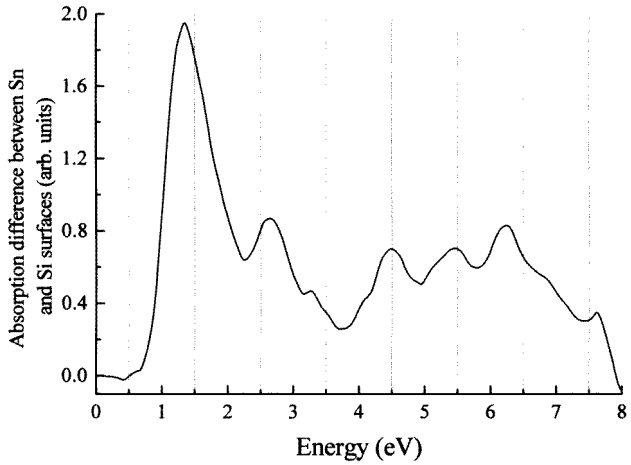

Figure 5. The calculated difference between the ϵ_2 for the Sn–Si(111)$\sqrt{3} \times \sqrt{3}$ and Sb–Si(111)$\sqrt{3} \times \sqrt{3}$ surfaces.

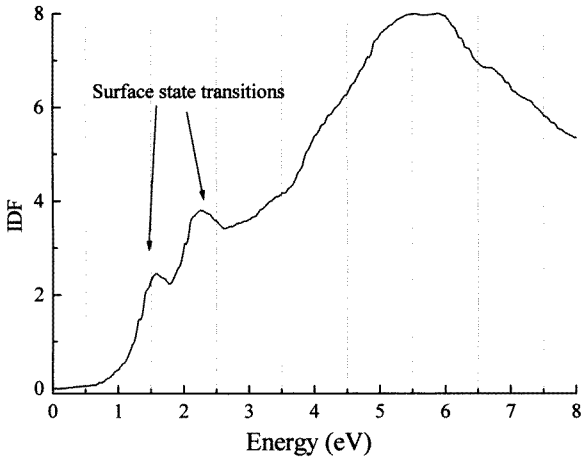

Figure 6. The imaginary part of the dielectric function (IDF), ϵ_2, for the Sb–Si(111)$\sqrt{3} \times \sqrt{3}$ surface.

Si(111)$\sqrt{3} \times \sqrt{3}$ surface. Also shown in figure 7(b) is the RAS spectrum for this surface. The main features of the two spectra occur at roughly the same energies affirming the fact that dielectric and reflectance anisotropies are closely related. Producing an ϵ_2-difference spectrum for Sb and Si reconstructed surfaces was not directly possible because the surface atomic density for the Sb–Si(111)$\sqrt{3} \times \sqrt{3}$ surface is different from that of the Si(111)$\sqrt{3} \times \sqrt{3}$ surface and also because the atom positions are very different (i.e. near T_1 sites for Sb adatoms and near a T_4 site for a Si adatom).

In performing these calculations we have also ignored transitions from surface states very close to the Fermi level. Thus even for the Sn surface where there is a high density of states at the Fermi energy, ϵ_2 has almost zero intensity below 1.0 eV.

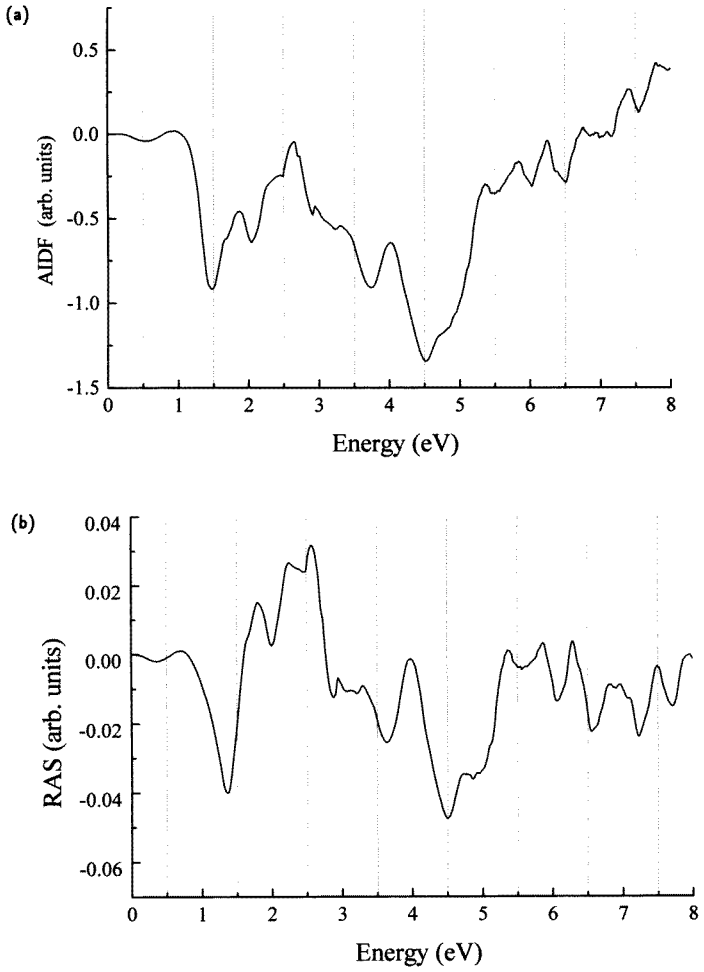

Figure 7. (a) The anisotropy in the imaginary part of the surface dielectric function (AIDF) for the Sb–Si(111)$\sqrt{3} \times \sqrt{3}$ surface as a function of energy. The two orthogonal polarizations considered are along the [110] and [$1\bar{1}2$] directions. (b) The RAS spectrum for the Sb–Si(111)$\sqrt{3} \times \sqrt{3}$ surface.

5. Conclusions

The SCTB technique has been used to calculate the electronic structure of the Sb– and Sn–Si(111)$\sqrt{3} \times \sqrt{3}$ reconstructed surfaces. The surface state energies are in good agreement with experimental findings. We have also calculated the imaginary part of the surface dielectric function for these surfaces using momentum matrix elements obtained from the electronic wave functions. The anisotropy of the surface dielectric functions have been calculated and compared with the RAS spectra for both surfaces. These calculated optical spectra show correlation with the detailed electronic structure, which in turn depends on the atomic configuration at the surface, and hence provide a useful tool in the study of surface structures. RAS and ellipsometry measurements for these surfaces are needed to provide a better understanding of the physics at these surfaces.

References

[1] Kittel C 1986 *Introduction to Solid State Physics* (New York: Wiley)
[2] Chung C Y and Schulman J N 1985 *Phys. Rev.* **31** 2069
[3] Rossow U, Frotscher U, Richter W, Wilhelm W and Zahn D 1993 *Surf. Sci.* **287+288** 718
[4] Richter W 1993 *Phil. Trans. R. Soc.* A **344** 453
[5] Scholz S M, Muller A B, Richter W, Zahn D R T, Westwood D I, Woolf D A and Williams R H 1992 *J. Vac. Sci. Technol.* B **10** 1710
[6] Kamiya I, Aspnes D E, Florez L T and Harbison J P 1992 *Phys. Rev.* B **46** 15 894
[7] Chang Y C and Aspnes D E 1990 *Phys. Rev.* B **41** 12 002
[8] Shen T H and Matthai C C 1993 *Surf. Sci.* **287+288** 627
[9] Griffiths C L, Anyele H T, Matthai C C, Cafolla A A and Williams R H 1993 *J. Vac. Sci. Technol.* B **11** 1559
[10] Moss D J, Ghahramani E, Sipe J E and van Driel H M 1986 *Phys. Rev.* B **34** 8758
[11] Aspnes D E and Studna A A 1983 *Phys. Rev.* B **27** 985
[12] Hybertsen M S and Louie S G 1986 *Phys. Rev.* B **34** 4033, 5390
[13] Shen T H and Matthai C C 1991 *J. Phys.: Condens. Matter* **3** 1528
[14] Matthai C C, Rees N V and Shen T H 1992 *Appl. Surf. Sci.* **56–58** 525
[15] Bisi O and Calandra C 1981 *J. Phys. C: Solid State Phys.* **14** 5479
[16] Bisi O, Chiao L W and Tu K N 1984 *Phys. Rev.* B **30** 4664
[17] Moore C E 1958 *Atomic Energy Levels* NBS Circular No 467, vols I, II and III (Washington, DC: US Government Printing Office)
[18] Harrison W A 1980 *Electronic Structure and the Properties of Solids* (San Francisco, CA: Freeman); 1973 *Phys. Rev.* B **8** 4487
[19] Wooten F 1972 *Optical Properties of Solids* (New York: Academic)
[20] Ichikawa T 1984 *Surf. Sci.* **140** 37
[21] Nogami J, Park Sang-Il and Quate C F 1988 *J. Vac. Sci. Technol.* A **7** 1919
[22] Conway K M, Macdonald J E, Norris C, Vleig E and van der Veen J F 1989 *Surf. Sci.* **215** 555
[23] Abukawa T, Park C Y and Kono S 1988 *Surf. Sci.* **201** L513
[24] Martenssen P, Meyer G, Amer N M, Kaxiras E and Pandey K C 1990 *Phys. Rev.* B **42** 7230
[25] Chelikowsky J R and Cohen M L 1976 *Phys. Rev.* B **14** 556
[26] Whittle R, McGovern I T, Hughes A, Shen T H and Matthai C C 1993 *J. Phys.: Condens. Matter* **5** 6555
[27] Kamiya I, Aspnes D E, Florez L T and Harbison J P 1992 *Phys. Rev.* B **46** 15 894
[28] Aspnes D E, Florez L T, Studna A A and Harbison J P 1990 *J. Vac. Sci. Technol.* B **8** 936
[29] Skriver H L 1984 *The LMTO Method* (New York: Springer)
[30] Kinoshita T, Ohta H, Enta Y, Yaegashi Y, Suzuki S and Kono S 1987 *J. Phys. Soc. Japan* **56** 4015
[31] Kinoshita T, Ohta H, Enta Y, Yaegashi Y, Suzuki S and Kono S 1988 *Surf. Sci.* **204** 405
[32] Hanke W and Sham L J 1980 *Phys. Rev.* B **21** 4656
[33] Engel G E and Farid B 1992 *Phys. Rev.* B **46** 15 812
[34] Selloni A, Marsella P and Del Sole R 1986 *Phys. Rev.* B **33** 8885
[35] Northrup J E 1986 *Phys. Rev. Lett.* **57** 154